Synchrotron Infrared Microspectroscopy Detecting the Evolution of Huntington's Disease Neuropathology and Suggesting Unique Correlates of Dysfunction in White versus Gray Brain Mat...

ARTICLE *in* ANALYTICAL CHEMISTRY · SEPTEMBER 2011

Impact Factor: 5.64 · DOI: 10.1021/ac201102p · Source: PubMed

9 AUTHORS, INCLUDING:

Bertrand Vileno
University of Strasbourg
23 PUBLICATIONS **374** CITATIONS
SEE PROFILE

László Forró
École Polytechnique Fédérale de Lausanne
207 PUBLICATIONS **5,560** CITATIONS
SEE PROFILE

Sylvia Jeney
École Polytechnique Fédérale de Lausanne
43 PUBLICATIONS **839** CITATIONS
SEE PROFILE

Published in final edited form as:
Anal Chem. 2011 October 15; 83(20): 7712–7720. doi:10.1021/ac201102p.

Synchrotron infrared micro-spectroscopy detects the evolution of Huntington's disease neuropathology and suggests unique correlates of dysfunction in white versus grey brain matter

Markus Bonda[1], **Valérie Perrin**[2], **Bertrand Vileno**[3], **Heike Runne**[2], **Ariane Kretlow**, **László Forró**[1], **Ruth Luthi-Carter**[2], **Lisa M. Miller**[4], and **Sylvia Jeney**[*,1]

[1]Laboratoire of Physics of Complex Matter, Ecole Polytechnique Fédérale de Lausanne (EPFL), CH-1015 Lausanne, Switzerland [2]Functional Neurogenomics Laboratory (LNGF), Faculté des sciences de la vie, Ecole Polytechnique Fédérale de Lausanne, Switzerland [3]Laboratoire POMAM, Institut de Chimie de Strasbourg, UMR7177 - CNRS-UDS, 67008 Strasbourg FRANCE [4]National Synchrotron Light Source, Brookhaven National Laboratory, Upton, NY 11973

Abstract

Huntington's disease (HD), caused by a mutation of the corresponding gene encoding the protein huntingtin (htt), is characterized by progressive deterioration of cognitive and motor functions, paralleled by extensive loss of striatal neurons. At the cellular level, pathogenesis involves an early and prolonged period of neuronal dysfunction followed by neuronal death. Understanding the molecular events driving these deleterious processes is critical to the successful development of therapies to slow down or halt the progression of the disease. Here, we examined biochemical processes in a HD *ex vivo* rat model, as well as in a HD model for cultured neurons using synchrotron-assisted Fourier transform infrared microspectroscopy (S-FTIRM). The model, based on lentiviral-mediated delivery of a fragment of the HD gene, expresses a mutant htt fragment in one brain hemisphere, and a wild-type htt fragment in the control hemisphere. S-FTIRM allowed for high spatial resolution and distinction between spectral features occurring in grey and white matter. We measured a higher content of β-sheet protein in the striatal grey matter exposed to mutant htt as early as 4 weeks following the initiation of mutant htt exposure. In contrast, white matter tracts did not exhibit any changes in protein structure, but surprisingly showed reduced content of unsaturated lipids and a significant increase in spectral features associated with phosphorylation. The former is reminiscent of changes consistent with a myelination deficiency, while the latter is characteristic of early pro-apoptotic events. These findings point to the utility of the label-free FTIRM method to follow mutant htt's β-sheet-rich transformation in striatal neurons *ex vivo*, provide further evidence for mutant htt amyloidogenesis *in vivo*, and demonstrate novel chemical features indicative of white matter changes in HD. Parallel studies in cultured neurons expressing the same htt fragments showed similar changes.

Keywords

Huntington's disease; polyglutamine; protein misfolding; phosphorylationbrain; neurons; infrared microspectroscopy

[*]To whom correspondence should be addressed .

INTRODUCTION

Huntington's disease (HD) is a genetic disorder characterized by progressive deterioration of cognitive and motor functions, paralleled by extensive loss of neurons, predominantly in the caudate nucleus and the putamen (striatum) of the brain.[1,2] In HD, a polymorphic cytosine-adenine-guanine (CAG) trinucleotide repeat in exon 1 of the HD gene is responsible for the polyglutamine (polyQ) stretch in the N-terminal of the huntingtin (htt) protein; the longer the polyQ stretch (starting at amino acid 18), the earlier its onset.[3,4] The formation of polyQ aggregates is hypothesized to be a stepwise process resulting in a parallel β-sheet fibrillar structure.[5–7] Recent work suggests also that not only the repeat length itself, but also the first 17 amino acids, may play a crucial role in regulating the conformational properties of htt.[8]

In vivo, fragments of the human N-terminal htt with varying polyQ expansions aggregate in striatal neurons and nucleate into nuclear and cytoplasmatic structures sometimes referred to as inclusion bodies (IBs).[9,10] In HD patients and many animal models of HD, IB formation precedes the onset of symptoms.[11] *In vitro*, the introduction of pre-formed htt inclusions into mammalian cells leads to subsequent cell death.[12] The blockade of neurite transport and sequestration of vital cellular proteins such as transcription factors are two of the possible ways in which inclusions may be toxic.[13,14] In the present work, we used a formerly well characterized genetic model of Huntington's disease (HD) based on lentiviral (LV)-mediated gene delivery to locally overexpress mutated htt in the striatum of adult rats.[15,16] To complement previous imunohistological analyses, we employed S-FTIRM for high spatial resolution mapping of HD-affected striatal tissue. The area of striatum expressing exogenous mutant htt fragment (htt171-82Q) was directly compared to the area of striatum expressing exogenous wild-type htt fragment (htt171-18Q). Brain slices were mapped at three different pathologic stages: 4, 6, and 8 weeks. In parallel, the lentiviral vectors expressing wild-type and mutant htt protein were used to infect rat primary striatal neuron cultures. In this *in vitro* model, the expression of wild type or mutated htt (htt171-18Q or htt171-82Q) can be achieved in the majority of neurons in the vicinity of the injection site.[16] Mutated htt produces a slowly progressive pathology characterized by the appearance of neuritic aggregates followed by intranuclear mutant htt accumulation, morphological anomalies of neurites, and loss of neurofilament expression. Cultures were infected with TRE-htt171-18Q or TRE-htt171-82Q LV, fixed at 1 and 1.5 weeks, and mapped by S-FTIRM. This allowed to localize and track the formation of aggregates in an *in vitro* system.

Infrared absorption peaks arise due to vibrational modes of atomic bonds presenting a dynamic dipole moment. Spectra are composed of characteristic bands that originate from absorption by the vibration of specific bonds. Since biomolecules such as proteins, lipids, nucleic acids have unique molecular assemblies, they have distinctly different infrared spectra. In the fine structure, infrared absorption also depends on the conformation of a molecule and so FTIR spectroscopy provides a chemical fingerprint of distinct tissue structures.[17,18] Analysis of protein conformation can be accomplished by means of the most sensitive amide I band. This vibrational mode originates from the C-O stretching of the amide group coupled to the in-phase bending of the N-H bond and the stretching of the C-N bond.[19] Its bands are found in the region between 1700 and 1600 cm^{-1}. Conformational changes of proteins have been detected in brain tissue affected by Alzheimer's disease[20,21] and scrapie.[22,23] In addition, vibrational spectroscopic imaging methods give an excellent chemical contrast, and can be utilized in this study for disentangling the biomolecular composition between the white and grey matter in brain tissue without the use of labels or stains.[24,25]

Over the past decade it was also shown that even small differences based on lipid composition, e.g. within grey matter and even brain sub-structures that are not easily identified by histology, can also be used for IR-based differentiation.[26,27] Furthermore, phosphorylation can be studied by FTIR by monitoring the phosphate stretching vibrations of the P-O double bond around 1237 and 1080 cm^{-1}.[28,29] Lipid unsaturation is a crucial indicator for other biochemical processes such as lipid peroxidization and is detectable by FTIRM. For instance, peroxidation by-products have been found in Alzheimer's disease human and mice brains that were spatially linked to regions with increased deposit of plaques.[27,30] Interestingly, lipid peroxidation was found to occur at early stages of the disease.[31]

EXPERIMENTAL SECTION

LV vector production

LV vectors encoding the first 171 amino acids of the human htt protein with 18 (18Q, wild-type) or 82 (82Q, mutated) polyQ repeats were produced in 293T cells, concentrated by ultracentrifugation, and resuspended in 1% bovine serum albumin in phosphate-buffered saline (PBS) as previously reported.[15,16] Viral particle content was defined by p24 antigen ELISA (RETROtek, Gentaur, Paris, France). Viral stocks were stored at −80°C until use.

In vivo HD model

All experiments were carried out in accordance with the European Community directive (86/609/EEC) for the care and use of laboratory animals. Adult female Wistar rats (Iffa Credo/Charles River, Les Oncins, France) were introduced into the experiment at a weight between 180-200 grams. The animals were housed in a controlled-temperature-room maintained on a 12 hrs day/night cycle, with food and water provided *ad libitum*. Concentrated viral stocks were thawed on ice and resuspended by repeated pipetting. htt171-18Q- or htt171-82Q-expressing lentiviral vectors were stereotactically injected into the striata of 8 rats anesthetized with ketamine (75 mg/kg i.p.) and xylazine (10 mg/kg i.p.) using a 34-gauge blunttipped needle linked to a Hamilton syringe (Hamilton, Reno, NV, USA) via a polyethylene catheter. The stereotactic coordinates used for the injection were: 0.5 mm rostral to bregma; 3 mm lateral to midline and 5 mm from the skull surface. The particle content of each concentrated virus was adjusted to 120′000 ng p24/ml. We injected 4 μl of viral suspension at a rate of 0.2 μl/min into the striatum via an automatic injector (Stoelting Co., Wood Dale, USA). The needle was left in place for 5 minutes after injection. The skin was closed with Autoclip wound clips (Phymep, Paris, France). Animals were injected with 4 μl of htt171-18Q in the left striatum and htt171-82Q on the right striatum (n = 2 per group). The animals were sacrificed 4, 6 and 8 weeks after injection using an overdose of sodium pentobarbital and transcardially perfused with a phosphate buffer solution (PB: 240 mM NaH2PO4=Na2HPO4, pH 7.4). The brains were removed and snap-frozen in isopentane on dry ice and stored at −80°C until further processing. Finally, brains were sectioned using a sledge cryomicrotome with a freezing stage of −20°C (SM2400, Leica Microsystems AG, Glattbrugg, Switzerland). Coronal sections of 7 μm throughout the entire striatum were mounted onto low-e IR slides (Crystran, UK) and transported within 10 days under humidity controlled atmosphere (20%-30%) to the National Synchrotron Light Source, Brookhaven National Laboratory (Upton, NY) for S-FTIRM mapping. Approximately 5 non-adjacent slices separated by at least 40 μm were studied per animal.

For immunohistochemical processing, sections of 25 μm were collected and stored in 96-well plates, free-floating in PBS supplemented with 0.12 μmol/l sodium azide. Staining was performed as previously described[32,33] for dopamine and cyclic adenosine monophosphate–regulated phosphoprotein with a molecular mass of 32 kDa (DARPP-32, 1:8,000, Chemicon

International, Temecula, CA) and with a rabbit polyclonal anti-ubiquitin antibody (Dako). DARPP-32, which regulates dopamine receptor signaling, is expressed in 96% of the striatal medium-sized spiny neurons and has been shown to be down-regulated in the present HD model.[15]

In vitro primary cell cultures

E16 rat striatal primary cultures were established through a previously described procedure.[34] Cells were plated on uncoated calcium fluoride (CaF_2) disks (13 mm diameter, 1 mm thickness, Crystran, UK) at a density of 150'000 cells per disk. On *in vitro* day 1 (DIV1), the cultures were infected with the htt171-18Q or htt171-82Q lentiviral vector (1/1 ratio; 15 ng p24 for each vector). On DIV 4, half the medium was replaced with freshly prepared neurobasal medium supplemented with 1% B27 (Gibco, Invitrogen, Basel Switzerland), 2% penicillin - streptavidin (10′000 U/ml, 10′000 μg/ml), 0.5 mM L-glutamine, and 15 mM KCl. Subsequently, half the medium was changed weekly. Cultures were fixed on CaF_2 disks with cold EtOH at 1 and 1.5 weeks after infection. Immunohistochemical staining for htt (mouse monoclonal 2B4, 1:200, a gift from Y. Trottier, CNRS/INSERMLP, Illkirch, France)[35] was performed as previously described.[32,33]

S-FTIRM data collection

The S-FTIRM experiments were conducted at Beamline U10B at the National Synchrotron Light Source, Brookhaven National Laboratory (Upton, NY). A Thermo Nicolet Magna 860 FTIR spectrometer, coupled to a Continuμm IR microscope (Thermo Nicolet, Madison, WI, USA), was used with synchrotron infrared light from the VUV-IR ring. The microscope was equipped with a 32x Schwarzschild objective/condenser pair, an adjustable rectangular aperture, and a liquid-nitrogen cooled mercury cadmium telluride detector (MCT-A, 50μm in size).[36,37] An automated X-Y mapping stage allowed sample scanning with a step accuracy of 1 μm.

Brain tissue slices—The aperture of the microscope was set to 10 × 10 μm^2 in order to optimize S/N ratio in the amide I and phosphate region, and achieve diffraction-limited spatial resolution of ~3-5 μm. An area of approximately 200 × 200 μm^2 was raster-scanned with a step size of 5 μm using Omnic software (ThermoNicolet). At each point, an absorbance spectrum was recorded in trans-reflection mode. Each spectrum was collected in the mid-infrared spectral range (4000-650 cm^{-1}) with a spectral resolution of 8 cm^{-1} and 64 scans were co-added. Happ-Genzel apodization and a zero-filling of level 2 were applied, resulting in approximately 1 data point per wavenumber. A background spectrum on a clean area of the low-e slide was also recorded by co-adding 256 scans. A total of approximately 9000 spectra were recorded per time point and brain side (82Q and 18Q).

Isolated neurons—Spectra of single neuronal cells, cultured on CaF_2 disks, were acquired in transmission mode. Neurons were identified by eye with optical microscopy at 320x magnification. Their x-y-coordinates on the sample stage were stored by the software so as to automatically approach the selected cells and collect their respective spectra. We used a 15 × 15 μm^2 aperture covering the whole neuronal cell body, a spectral resolution of 8 cm^{-1}, a spectral range between 4000 and 700 cm^{-1}, and 64 scans were added together to enhance the S/N ratio. Prior to each experiment, a background spectrum was taken consisting of 256 combined spectra from a clean, cell-free place on the CaF_2 disk. Approximately 200 neurons were measured per condition.

Data analysis

Brain tissue slices—Infrared profile images were generated by dividing one area of a given spectral range by another one and then displaying the ratio in a false color image, also called map. In an absorption spectrum, the integrated area of a spectral region is proportional to the concentration of the feature associated with it. The mapping analysis was accomplished using Omnic 7.4 (Thermo Fisher Scientific Inc.). A linear baseline was used to correct for the decaying synchrotron beam current over time. Pixels from white vs. grey matter were separated based on lipid content, in order to obtain independent statistics for each tissue type present in the striatum. By calculating the lipid/protein ratio (3000-2800 cm^{-1}/1700-1600 cm^{-1}), we clearly distinguished between white and grey matter in each map. Grey matter is typically composed of 33% lipids and 55% protein,[38] which yields a lipid/protein ratio of ≈0.6. Conversely, white matter is composed of 55% lipids and 40% protein,[38] which corresponds to a higher lipid/protein ratio of ≈1.4. After S/N quality testing to remove pixels with low absorbance and/or high noise, pixels from the grey matter were separated from white matter pixels based on a lipid/protein ratio threshold value of 1.05. All custom-made analysis software was written in Mathematica (Wolfram Research, Inc., Champaign, Ill, USA).

After separating white from grey pixels, the following parameters were analyzed for each pixel:

- **i.** Lipid content (lipid/protein ratio): The relative lipid content was determined by integrating the C-H stretching vibration region of the spectra from 3000-2800 cm^{-1} using a baseline with the same limits. This band includes stretching vibrations from the aliphatic methylene band ($-CH_2$ antisymmetric stretching at 2920 cm^{-1} and symmetric stretching at 2850 cm^{-1}), and the methylene group ($-CH_3$ antisymmetric stretching at 2957 cm^{-1} and symmetric stretching at 2872 cm^{-1}).[17] The lipid content was normalized to protein content (area: 1700-1600 cm^{-1}; linear baseline: 1760-1480 cm^{-1}) to account for variations in tissue thickness.
- **ii.** β-sheet content (β-sheet/total protein ratio): The amide I band, between 1700 and 1600 cm^{-1} arises from the stretching modes of C=O amide carbonyl groups in the protein backbone and is sensitive to protein conformation. The content of β-sheet structure in the tissue was determined by integration from 1628-1624 cm^{-1}.[20,22] Wavenumber regions were chosen to be narrow to prevent overlapping with neighboring spectral features. The β-sheet content was normalized to total protein content as described in (i) to account for variations in tissue thickness.
- **iii.** Phosphorylation (phosphate/lipid ratio). In the phosphate-stretching region, we quantified phosphorylation by integrating the area of the antisymmetric P=O double bond stretching band, 1240-1235 cm^{-1} (linear baseline: 1280-1190 cm^{-1}) and normalizing by the lipid band area described in (i). This band is sufficiently separated from the amide III band at 1299 cm^{-1} for accurate analysis.[17,39,40]
- **iv.** Olefinic content (olefinic/total lipid) was determined by integrating the 3012 cm^{-1} =C-H stretching mode from 3020 to 3000 cm^{-1}.[27,40-42] The baseline range was also 3020-3000 cm^{-1}. The peak intensity at 3012 cm^{-1} is proportional to the amount of unsaturated lipid in the tissue. The olefinic content was normalized to total lipid content with the parameters described in (i).

Once the parameters were calculated for each condition, histograms were generated from all pixels for each time point. All distributions were normalized by the total area of the histogram yielding the density, such that:

$$\sum_{i}^{N} f(x_i)\,(b[i+1] - b[i]) = 1$$

(*i* is the index running from *0* to the *N*th bin of the histogram, $f(x_i)$ are the frequencies or counts in a given bin, and *b[i]* are the bin limits) using the program R (http://www.r-project.org/). The total number of pixels that were measured per condition was on average 7500 spectra in grey matter, and 1500 in white matter.

Isolated neurons—Spectra obtained from a series of single cell measurements were processed using a macro written in Macros\Basic (Thermo Fisher Scientific, Waltham, MA, USA) and Omnic 7.4. The same spectral regions, baselines, and normalizations that were used for the brain tissue analysis described above were used for the isolated neurons. The program R was used again for compiling histograms for any spectral ratio calculated with the Omnic macro.

RESULTS AND DISCUSSION

Brain tissue experiments

The left and right striata of the rat brain, injected with Lentiviral vectors encoding the first 171 amino acids of wild-type (htt171-18Q) or, respectively, mutant htt(htt171-82Q) are shown Figure 1A. As expected from ealier studies[15,33], expression of mutated htt leads to the progressive development of a pathology characterized by sequential appearance of ubiquitinated htt inclusions, cellular dysfunction accompanied by the loss of the GABAergic projection neuron marker DARPP-32 and neuronal nuclei staining (Figure 1B), and finally neuronal death. 4 weeks post-injection, mutant htt-exposed cells are distinguished by some loss of DARPP-32 expression and progressive accumulation of htt aggregates.[15] At 8 weeks post LV injection, various neuronal markers are lost and a pronounced accumulation of htt aggregates is present (Figure 1C).

In order to establish the early neuropathology caused by mutant htt in rat brain, we applied S-FTIRM to striatal tissues exposed to mutant versus wild-type htt fragments *in vivo*. In optical microscopy, the white matter tracts appear as darker patches dispersed within the grey matter tissue (Figure 2A). The characteristic IR-spectra shown in Figure 2B confirm that grey matter is composed of protein-rich neuronal cell bodies, whereas white matter contains mostly fatty myelin-wrapped axons. The corresponding map displayed in Figure 2C highlights the clear separation between white and grey matter. The main advantage of the presented approach is that grey and white matters appear together in each examined brain section. Furthermore, both brain sides, 18Q and 82Q, were analyzed in parallel and within the same animal (Figures 3A and 3B).

Since lipid content is significantly higher in the white matter, an infrared image representing the lipid/protein ratio was used to clearly distinguish white from grey matter. As can be seen in Figures 3C and 3D, the white matter regions, circled with black lines, have a high lipid/protein ratio, indicated by red and yellow pixels. In Figures 3E and 3F, we compared the β-sheet content between the diseased and control tissue at 8 weeks after infection. Here, we clearly see a higher β-sheet content in the grey matter of the diseased side, as indicated by many more green to red pixels. Figures 3G and 3H display the ratio between the antisymmetric phosphate stretching mode (around 1237 cm^{-1}) and total lipid content, where a larger number of red and yellow pixels indicates a higher concentration of phosphate groups in the grey matter of the 82Q side of the striatum, possibly due to elevated protein and/or lipid phosphorylation. The spatial distribution of olefinic lipids normalized to the

total lipid content, associated with unsaturated fatty acids, are displayed by Figures 3I and 3J. On the 82Q side, the white matter areas indicate a much lower olefinic content than the grey matter. The part of the striatum infected with the wild-type vector similarly displays various red pixels in grey matter.

To elucidate whether grey and white matter in the striatum are affected differently by HD, we compared, separately for grey and white matter, changes in all recorded IR maps with respect to protein structure, phosphorylation, and unsaturated lipid content. We obtained 3 statistical distributions for each spectral feature investigated at every time point. In Figure 4, distributions in grey matter (main frames) are displayed for the relative β-sheet content as a function of the studied time points. At the first time point of 4 weeks, the spectral distributions of both 18Q and 82Q grey matter showed a similar β-sheet content. After 6 weeks, a narrower distribution was observed in the 82Q spectra with a small fraction of the distribution appearing at higher values, around 0.04 compared to 18Q. By 8 weeks, a dramatic broadening of the β-sheet content became apparent in the 82Q distribution, where a significant number of pixels had a higher β-sheet content than the 18Q distribution. Conversely, no significant differences in β-sheet content were observed between 18Q and 82Q in the white matter at any time point, as shown in the insets.

In order to study phosphorylation, the antisymmetric phosphate stretching mode[40] was analyzed, as shown in Figure 5A. In the white mattter (main frames) at 4 and 6 weeks after infection, no differences were observed in the 82Q vs. 18Q distributions. After 8 weeks, however, concomitant with the evolution of high β-sheet content in grey matter, the 82Q phosphate distribution broadened dramatically with a large number of pixels exhibiting a high level of phosphorylation. In contrast, very little differences were observed between 82Q and 18Q in the grey matter over the time course of the experiment (insets).

The content of unsaturated fatty acids was monitored by analyzing the olefinic stretching vibration at 3012 cm^{-1} (Figure 5B). 4 weeks after infection, the 82Q and the 18Q statistical distributions were equal in white matter (main frames). As of 6 weeks, we observed a lag in the 82Q distribution compared to the control side of the brain. A reduction in unsaturated lipids in the diseased side of the brain may have diverse origins one of which is lipid peroxidation in the white matter.[27] The corresponding distributions in grey matter exhibited very little differences between 4 and 8 weeks after infection (insets). In order to assess statistical differences between all studied features, we performed a pairwise analysis of left and right brain side, through a Mann-Whitney U test. In the cases were the p-values were found to be smaller than 5.10^{-2}, differences between the compared distribution were considered as significant. Changes in the β-sheet content in the grey matter, as well as a reduction of unsaturated lipids in the white matter appeared to be significant already from the very first time point on, while the observed increase in phosphorylation in white matter were significant after 8 weeks.

Neurons – *in vitro* experiments

Primary neurons were exposed to the same htt171-82Q fragment used in the *ex vivo* experiment, but using the stronger tTA/TRE expression system so as to have a more rapid neurpathologic phenotype. Negative control cells were exposed to an htt171-18Q fragment. We expected these *in vitro* experiments to produce results similar to those observed in grey matter tissue samples since the main component of grey matter is neurons. The investigated time points *in vitro* were 1 and 1.5 weeks, which represent early time points course similar to the progression of the disease in the tissue (a state of dysfunction upstream of neuronal death). In the histograms associated with normalized β-sheet content (Figure 6), β-sheet distributions were shifted to higher values in cells, ranging from 0.035-0.055 as compared to 0.025-0.050 in tissue, consistent with the higher expression of mutant htt in the cellular

system. Moreover, the 82Q cell distribution exhibited a higher β-sheet content at the first time point, which did not evolve further. It is therefore likely that the most severely diseased cells detached from their CaF_2 substrate soon after htt171-82Q accumulation. While, in general, the histograms of the cells are more scattered than those of tissue due to a smaller number of spectra analyzed, the main observation of increase β-sheet content is qualitatively similar to the *in vivo* result. A standard Mann-Whitney U test confirmed again statistical relevance of our results.

Several observations are evident from the experimental results of this study. First, S-FTIRM reveals an increased β-sheet content as early as 4 weeks in the grey matter of a rat model of HD. This increase can be correlated to the accumulation of htt aggregates in neuronal nuclei and the neuropil.[15,43] Indeed, *in vitro* studies showed that polyQ aggregates are mainly composed of parallel in-register β -sheets.[44,45] Previous work has used thioflavin S, antibodies, dynamic light scattering or electron microscopy to detect mutant htt aggregates.[4–12,44,46,47]

The infrared images also show a sharp increase in phosphorylated molecules in the white matter tracts composed of myelinated axons crossing the striatum 8 weeks after injection of the LV. Parallel phosphate histograms of grey tissue expressing htt171-18Q or htt171-82Q confirm that phosphorylation occurs in the white matter in the same time frame as the significant increase in β-sheet content in grey matter. Such an increase of phosphorylation may be interpreted as a signaling response to mutant htt protein accumulation-induced cell stress. A current hypothesis for the origin of this cellular stress is that mutated htt follows a mechanism of toxic gain of function[13] that may arise from aggregation itself or the interaction of mutated htt with cellular processes. Indeed, impaired proteosomal function, altered gene transcription, deficiencies in dopaminergic modulation in cell signaling,[48] and in particular activation of the apoptotic cascade have been found to be implicated in pathogenesis of HD models. In this context, it has been shown *in vitro*[49,50] and *ex vivo*[43] that expanded polyQ proteins induce a stress response involving the JunN-terminal kinase pathway and hence activating phosphorylation cascades. However, at the present time, we cannot distinguish as to whether this is a response of the neuronal axons themselves or a change in the surrounding myelin.

This change is also accompanied by a significant decrease in unsaturated fatty acids in the myelin-rich white matter of the 82Q striatum. Polyunsaturated lipids in the brain have a role in supporting the structure, fluidity, and function of cellular and subcellular membranes and myelin. They are essential to brain functions such as signal transduction and cell survival.[51] However, unsaturated lipids are most susceptible to degradation through free radicals and peroxidation, and the results shown here suggest evidence for lipid damage in the white matter in the HD model.

CONCLUSION

This study showed that infrared microspectroscopy is a valuable tool for high-resolution analysis of HD tissue, which allows simultaneous analysis of neuron-rich grey matter or from myelin and axon-rich white matter tracts present in the striatum. The proposed methodology provides new insights on biochemical processes occurring within a non-fixed brain sample, hence in their original environment and arrangement. In contrast to more standard histological, immunohistochemical or ultrastructural studies of protein aggregation in HD,[15,33,52] molecular transformations can be tracked without staining or further chemical modifications, yielding a non-biased chemical composition of the studied structures. Additionally, the technique of mapping allows to precisely localize the studied features. In particular, we were able to clearly distinguish spectral features characteristic of grey matter

and white matter tracts in brain tissue. Since there have been very little quantitative structural data reported to date on mutant htt aggregation in intact brain tissue in the literature, and none from this particular lentiviral model, it is not possible to make direct head-to-head comparisons to other methods. However, we plan to conduct future experiments to assess the specific molecular species and determinants that contribute to the features we have detected with S-FTIRM using a variety of techniques.

S-FTIRM analysis demonstrated an increase in β-sheet content, which we relate to the formation of htt aggregates in striatal grey matter. In parallel, increased phosphorylation and decreased unsaturated fatty acids were detected in striatal white matter, comprising neuronal axons and myelin sheaths formed by oligodendrocytes. While the exact mechanism is yet to be elucidated, these results indicate that protein aggregation and IB formation come along with a reduction of unsaturated lipid content in the brain, impacting brain growth, membrane fluidity, signal transduction, and cognitive development. These results provide new molecular evidence for white matter abnormalities and motivate further study of the relationships between intraneuronal dysfunction and myelin-related changes in HD. Understanding the biological basis for these changes may shed light on previously described white matter volume loss in human HD brain.[53]

Acknowledgments

This work was supported by grants to MB from the Swiss National Science Foundation through project No. 200021-113529 and to SJ through the NCCR for nanoscale science. We would like to acknowledge the technical assistance of Randy Smith and thank Dr. Tamara Serededina for photomicrographs of cultured neurons. This work is supported by the National Institutes of Health grant R01-GM66873 (LMM). The NSLS is supported by the United States Department of Energy under contract DE-AC02-98CH10886.8.

REFERENCES

[1]. Folstein, S. Huntington’s disease: a disorder of families. Johns Hopkins University Press; Baltimore: 1989. p. 1-64.

[2]. Wexler NS, Rose EA, Housman DE. Annu. Rev. Neurosci. 1991; 14:503–529. [PubMed: 1827708]

[3]. The Huntington’s Disease Collaborative Research Group. Cell. 1993; 72:971–83. [PubMed: 8458085]

[4]. Paulson HL. Brain Pathol. 2000; 10:293–299. [PubMed: 10764049]

[5]. Perutz MF, Pope BJ, Owen D, Wanker EE, Scherzinger E. Proc. Natl. Acad. Sci. U S A. 2002; 99:5596–600. [PubMed: 11960015]

[6]. Wetzel R. Structure. 2002; 10:1031–6. [PubMed: 12176381]

[7]. Ross CA, Poirier MA, Wanker EE, Amzel M. Proc. Natl. Acad. Sci. U S A. 2003; 100:1–3. [PubMed: 12509507]

[8]. Tam S, Spiess C, Auyeung W, Joachimiak L, Chen B, Poirier MA, Frydman J. Nat. Struct. Mol. Biol. 2009; 16:1279–85. [PubMed: 19915590]

[9]. Davies SW, Turmaine M, Cozens BA, DiFiglia M, Sharp AH, Ross CA, Scherzinger E, Wanker EE, Mangiarini L, Bates GP. Cell. 1997; 90:537–548. [PubMed: 9267033]

[10]. DiFiglia M, Sapp E, Chase KO, Davies SW, Bates GP, Vonsattel JP, Aronin N. Science. 1997; 277:1990–3. [PubMed: 9302293]

[11]. Gutekunst CA, Li SH, Yi H, Mulroy JS, Kuemmerle S, Jones R, Rye D, Ferrante RJ, Hersch SM, Li XJ. J. Neurosci. 1999; 19:2522–2534. [PubMed: 10087066]

[12]. Yang W, Dunlap JR, Andrews RB, Wetzel R. Hum. Mol. Genet. 2002; 11:2905–17. [PubMed: 12393802]

[13]. Cattaneo E, Rigamonti D, Goffredo D, Zuccato C, Squitieri F, Sipione S. Trends Neurosci. 2001; 24:182–8. [PubMed: 11182459]

[14]. Petersén A, Mani K, Brundin P. Exp. Neurol. 1999; 157:1–18. [PubMed: 10222105]

[15]. de Almeida LP, Ross CA, Zala D, Aebischer P, Déglon N. J. Neurosci. 2002; 22:3473–83. [PubMed: 11978824]

[16]. Rudinskiy N, Kaneko YA, Beesen AA, Gokce O, Régulier E, Déglon N, Luthi-Carter R. J. Neurochem. 2009; 111:460–72. [PubMed: 19686238]

[17]. Wetzel DL, LeVine SM. Science. 1999; 285:1224–5. [PubMed: 10484732]

[18]. Stuart, B. Infrared spectroscopy: Fundamentals and Applications. Wiley; London: 2004.

[19]. Surewicz WK, Mantsch HH, Chapman D. Biochemistry. 1993; 32:389–94. [PubMed: 8422346]

[20]. Choo LP, Wetzel DL, Halliday WC, Jackson M, LeVine SM, Mantsch HH. Biophys. J. 1996; 71:1672–9. [PubMed: 8889145]

[21]. Miller LM, Wang Q, Telivala TP, Smith RJ, Lanzirotti A, Miklossy J. J. Struct. Biol. 2006; 155:30–37. [PubMed: 16325427]

[22]. Kneipp J, Miller LM, Joncic M, Kittel M, Lasch P, Beekes M, Naumann D. Biochim. Biophys. Acta. 2003; 1639:152–8. [PubMed: 14636946]

[23]. Kretlow A, Wang Q, Beekes M, Naumann D, Miller LM. Biochim. Biophys. Acta. 2008; 1782:559–65. [PubMed: 18625306]

[24]. Levine SM, Wetzel DLB. Appl. Spectrosc. Rev. 1993; 28:385–412.

[25]. Lewis EN, Gorbach AM, Marcott C, Levin I. W. a. Appl. Spectrosc. 1996; 50:263–269.

[26]. Kneipp J, Beekes M, Lasch P, Naumann D. J. Neurosci. 2002; 22:2989–97. [PubMed: 11943801]

[27]. Leskovjan AC, Kretlow A, Miller LM. Anal. Chem. 2010; 82:2711–6. [PubMed: 20187625]

[28]. Amaral IF, Granja PL, Barbosa MA. J Biomater Sci Polym Ed. 2005; 16:1575–93. [PubMed: 16366338]

[29]. Vileno B, Jeney S, Sienkiewicz A, Marcoux PR, Miller LM, Forró L. Biophys. Chem. 2010; 152:164–9. [PubMed: 20970241]

[30]. Sayre LM, Zelasko DA, Harris PLR, Perry G, Salomon RG, Smith MA. J. Neurochem. 1997; 68:2092–2097. [PubMed: 9109537]

[31]. Williams TI, Lynn BC, Markesbery WR, Lovell MA. Neurobiol. Aging. 2006; 27:1094–9. [PubMed: 15993986]

[32]. Bensadoun JC, de Almeida LP, Dreano M, Aebischer P, Deglon N. Eur. J. Neurosci. 2001; 14:1753–1761. [PubMed: 11860469]

[33]. Perrin V, Régulier E, Abbas-Terki T, Hassig R, Brouillet E, Aebischer P, Luthi-Carter R, Déglon N. Mol. Ther. 2007; 15:903–911. [PubMed: 17375066]

[34]. Zala D, Benchoua A, Brouillet E, Perrin V, Gaillard M-C, Zurn AD, Aebischer P, Déglon N. Neurobiol. Dis. 2005; 20:785–98. [PubMed: 16006135]

[35]. Abbas-Terki T, Donze O, Briand PA, Picard D. Mol. Cell Biol. 2001; 21:7569–7575. [PubMed: 11604493]

[36]. Miller LM, Dumas P, Jamin N, Teillaud J-L, Miklossy J, Forró L. Rev. Sci. Instr. 2002; 73:1357–1360.

[37]. Miller LM, Smith RJ. Vib. Spectrosc. 2005; 38:237–240.

[38]. Norton, WT.; Cammer, W. Isolation and characterization of myelin. 2nd ed. Morell, P., editor. Myelin; Plenum; New York: 1984.

[39]. Mantsch HH, McElhaney RN. Chem. Phys. Lipids. 1991; 57:213–226. [PubMed: 2054905]

[40]. Lasch P, Boese M, Pacifico A, Diem M. Vib. Spectrosc. 2002; 28:147–157.

[41]. Liu K-Z, Bose R, Mantsch HH. Vib. Spectrosc. 2002; 28:131–136.

[42]. Severcan F, Gorgulu G, Gorgulu ST, Guray T. Anal. Biochem. 2005; 339:36–40. [PubMed: 15766707]

[43]. Perrin V, Dufour N, Raoul C, Hassig R, Brouillet E, Aebischer P, Luthi-Carter R, Déglon N. Exp. Neurol. 2009; 215:191–200. [PubMed: 19022249]

[44]. Scherzinger E, Sittler A, Schweiger K, Heiser V, Lurz R, Hasenbank R, Bates GP, Lehrach H, Wanker EE. Proc. Natl. Acad. Sci. U S A. 1999; 96:4604–4609. [PubMed: 10200309]

[45]. Wickner RB, Dyda F, Tycko R. Proc. Natl. Acad. Sci. U S A. 2008; 105:2403–2408. [PubMed: 18268327]

[46]. Scherzinger E, Lurz R, Turmaine M, Mangiarini L, Hollenbach B, Hasenbank R, Bates GP, Davies SW, Lehrach H, Wanker EE. Cell. 1997; 90:549–558. [PubMed: 9267034]

[47]. Georgalis Y, Starikov EB, Hollenbach B, Lurz R, Scherzinger E, Saenger W, Lehrach H, Wanker EE. Proc. Natl. Acad. Sci. U S A. 1998; 95:6118–6121. [PubMed: 9600927]

[48]. Bibb JA, Yan Z, Svenningsson P, Snyder GL, Pieribone VA, Horiuchi A, Nairn AC, Messer A, Greengard P. Proc. Natl. Acad. Sci. U S A. 2000; 97:6809–6814. [PubMed: 10829080]

[49]. Liu YF, Dorow D, Marshall J. J. Biol. Chem. 2000; 275:19035–19040. [PubMed: 10801775]

[50]. Merienne K, Helmlinger D, Perkin GR, Devys D, Trottier Y. J Biol. Chem. 2003; 278:16957–16967. [PubMed: 12598532]

[51]. Sastry PS. Prog. Lipid Res. 1985; 24:69–176. [PubMed: 3916238]

[52]. Díaz-Hernández M, Moreno-Herrero F, Gómez-Ramos P, Morán MA, Ferrer I, Baró AM, Avila J, Hernández F, Lucas JJ. J. Neurosci. 2004; 24:9361–9371. [PubMed: 15496672]

[53]. Ciarmiello A, Cannella M, Lastoria S, Simonelli M, Frati L, Rubinsztein DC, Squitieri F. J. Nucl. Med. 2006; 47:215–222. [PubMed: 16455626]

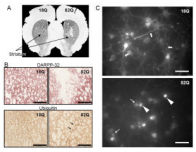

Figure 1.

HD-like neuropathology after local expression of mutant htt in rat brain. (A) Brain slice of an adult rat injected with htt171-18Q in the left (18Q) and with htt171-82Q in the right (82Q) striatum. (B) Images of DARPP-32- and ubiquitin-immunostained brain sections after exposure to htt171-18Q and htt171-82Q. htt171-82Q pathology is characterized by DARPP-32 depletion (top right panel) and the formation of htt- and ubiquitin-positive inclusions (bottom right panel, small arrows) after 8 weeks expression in vivo. Scale bars correspond to 500 μm. (C) In primary striatal neurons, htt immunoreactivity in 82Q compared to 18Q cells reveals the nuclear accumulation of htt (indicated by larger arrowheads on bottom panel) and aggregated mutant htt (indicated by small arrows bottom panel) and the loss of htt from the extranuclear compartment, for example neurites, as compared to the 18Q cells (whose stained neurites are indicated by rectangular arrows in top panel). Scale bars correspond to 25 μm.

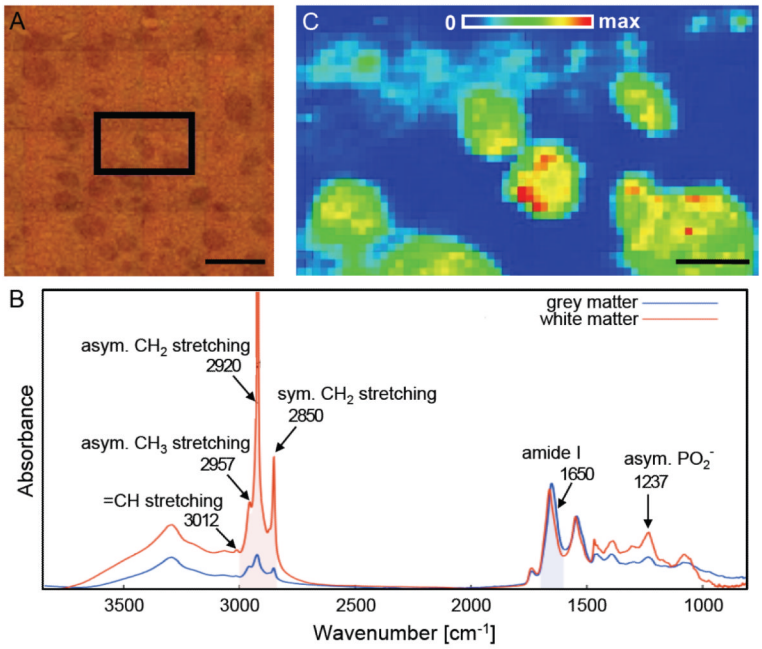

Figure 2.

Discrimination between grey and white matter: (A) Optical image of the part of the striatum selected to be mapped by S-FTIRM (black square). The white matter tracts appear as darker irregular patches. Scale bar = 200 μm. (B) Characteristic IR spectrum taken in the grey (blue line) and white matter (red line) of the striatal region. The region indicating lipid content is shaded red, whereas the amide I protein band is shaded blue. (C) Corresponding S-FTIRM map of the lipid content (integrated over 3000-2800 cm^{-1}) relative to the amide I protein band (1700-1600 cm^{-1}). The areas of higher lipid content (green to red) clearly match the darker regions in (A). The white matter tracts can hence be precisely distinguished from the surrounding grey matter by their high lipid content. Scale bar = 50 μm.

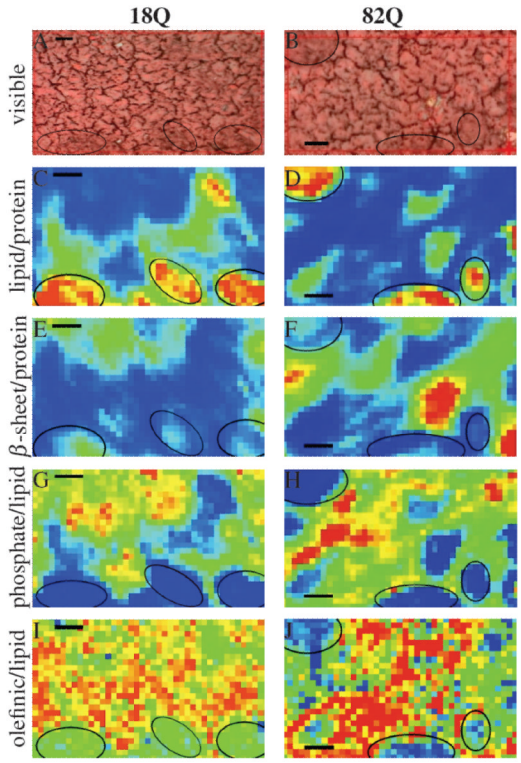

Figure 3.

S-FTIRM maps of the 18Q (left column) and 82Q (right column) sides of the striatum at 8 weeks. (A) and (B) visible micrographs. (C) and (D) lipid / protein profile to distinguish between grey and white matter. White matter is indicated by the black circles in all panels; (E) and (F) β-sheet / total protein profile; (G) and (H) antisymmetric phosphate stretching / total lipid profile. (I) and (J) olefinic lipid / total lipid profile. Scale bars are 25 μ for all panels, and color scales are kept the same among all maps of the same spectral parameter for comparison (blue = min, red = max).

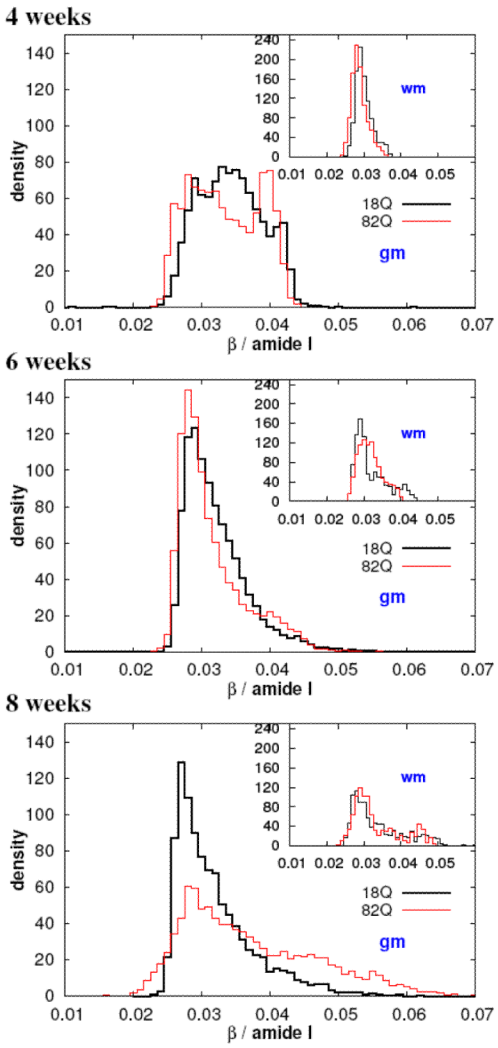

Figure 4.

Histograms in grey matter (gm, main panels) and white matter (wm, insets) calculated to follow the time course of β-sheet content in the striatum of the HD model *ex vivo* at time points 4, 6, and 8 weeks after infection with the LV. Statistical distributions from the 18Q side (control) are black and those from the 82Q (diseased) are drawn in red. The x-axis indicates the β-sheet / total protein content and the y-axis indicates the statistical density. The histograms in grey matter were calculated from ca. 7500 spectra per time point while those in the white matter from at least 400 per time point.

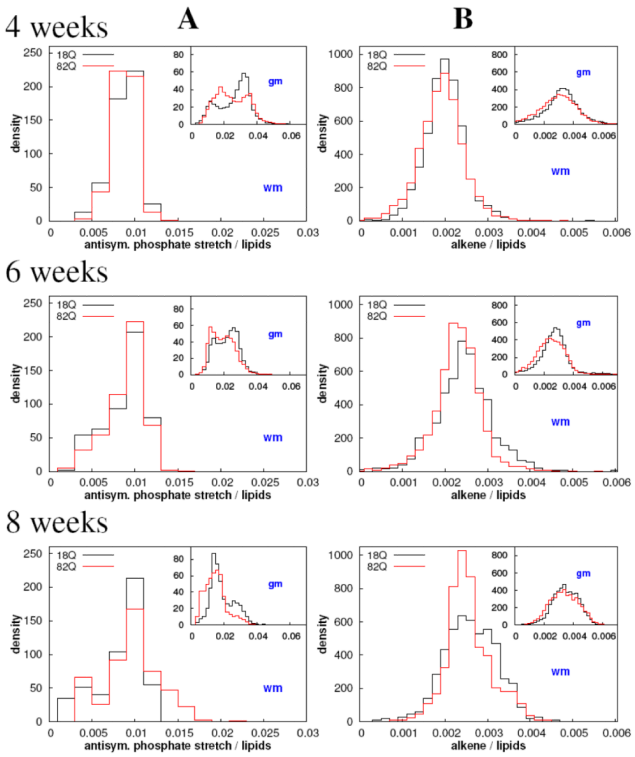

Figure 5.

Histograms in white matter (wm, main panels) and grey matter (gm, insets) calculated to follow the time course of phosphorylation (A) and olefinic lipids (B) in the striatum of the HD model *ex vivo* at time points 4, 6, and 8 weeks after infection with the LV. Statistical distributions from the 18Q side (control) are black and those from the 82Q (diseased) are drawn in red. The x-axis indicates the phosphate / lipid ratio (A) or the olefinic lipid / total lipid ratio (B). The y-axis denotes the statistical density. The histograms in grey matter were calculated from ca. 7500 spectra per time point, those in white matter from at least 400 per time point.

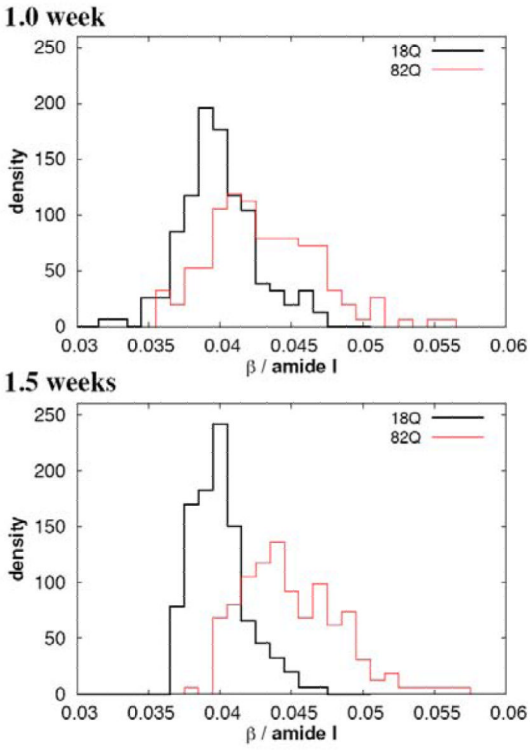

Figure 6.

Histograms calculated to follow the time course of HD *in vitro* at time points 1.0, 1.5 weeks. Evolution of β-sheet content relative to the total protein content of control (black) and diseased (red) neurons. The x- and y-axes are the same as in Figure 5. Histograms were calculated from ~ 200 spectra , corresponding to the same amount of cells per timepoint.